

Artificial Cells, Nanomedicine, and Biotechnology

An International Journal

ISSN: 2169-1401 (Print) 2169-141X (Online) Journal homepage: <https://www.tandfonline.com/loi/ianb20>

Stem cells combined 3D electrospun nanofibrous and macrochannelled matrices: a preliminary approach in repair of rat cranial bones

İsmail Alper İšođlu, Nimet Bölgen, Petek Korkusuz, İbrahim Vargel, Hakan Hamdi Çelik, Emine Kılıç, Elif Güzel, Tarık Çavuşođlu, Duygu Uçkan & Erhan Pişkin

To cite this article: İsmail Alper İšođlu, Nimet Bölgen, Petek Korkusuz, İbrahim Vargel, Hakan Hamdi Çelik, Emine Kılıç, Elif Güzel, Tarık Çavuşođlu, Duygu Uçkan & Erhan Pişkin (2019) Stem cells combined 3D electrospun nanofibrous and macrochannelled matrices: a preliminary approach in repair of rat cranial bones, *Artificial Cells, Nanomedicine, and Biotechnology*, 47:1, 1094-1100, DOI: [10.1080/21691401.2019.1593850](https://doi.org/10.1080/21691401.2019.1593850)

To link to this article: <https://doi.org/10.1080/21691401.2019.1593850>



© 2019 The Author(s). Published by Informa UK Limited, trading as Taylor & Francis Group.



Published online: 03 Apr 2019.



Submit your article to this journal [↗](#)



Article views: 384



View Crossmark data [↗](#)

Stem cells combined 3D electrospun nanofibrous and macrochannelled matrices: a preliminary approach in repair of rat cranial bones

İsmail Alper İsoğlu^a, Nimet Bölgen^b, Petek Korkusuz^c, İbrahim Vargel^{d*}, Hakan Hamdi Çelik^e, Emine Kılıç^f, Elif Güzel^g, Tarık Çavuşoğlu^h, Duygu Uçkan^f and Erhan Pişkinⁱ

^aFaculty of Life and Natural Sciences, Department of Bioengineering, Abdullah Gül University, Kayseri, Turkey; ^bFaculty of Engineering, Department of Chemical Engineering, Mersin University, Mersin, Turkey; ^cFaculty of Medicine, Department of Histology and Embryology, Hacettepe University, Ankara, Turkey; ^dFaculty of Medicine, Department of Plastics and Reconstructive Surgery, Hacettepe University, Ankara, Turkey; ^eFaculty of Medicine, Department of Anatomy, Hacettepe University, Ankara, Turkey; ^fFaculty of Medicine, Department of Pediatric Hematology – Bone Marrow Transplantation Unit and PEDI-STEM Stem Cell Research Centre, Hacettepe University, Ankara, Turkey; ^gCerrahpaşa Medical Faculty, Department of Histology and Embryology, İstanbul University-Cerrahpaşa, İstanbul, Turkey; ^hFaculty of Medicine, Department of Plastics and Reconstructive Surgery, Kırıkkale University, Kırıkkale, Turkey; ⁱCyberpark, Bilkent, Nanobiyomedtek Biyomedikal ve Biyoteknoloji San.Tic.Ltd.Şti., Ankara, Turkey

ABSTRACT

Repair of cranial bone defects is an important problem in the clinical area. The use of scaffolds combined with stem cells has become a focus in the reconstruction of critical-sized bone defects. Electrospinning became a very attracting method in the preparation of tissue engineering scaffolds in the last decade, due to the unique nanofibrous structure of the electrospun matrices. However, they have a limitation for three dimensional (3D) applications, due to their two-dimensional structure and pore size which is smaller than a cellular diameter which cannot allow cell migration within the structure. In this study, electrospun poly(ϵ -caprolactone) (PCL) membranes were spirally wounded to prepare 3D matrices composed of nanofibers and macrochannels. Mesenchymal stromal/stem cells were injected inside the scaffolds after the constructs were implanted in the cranial bone defects in rats. New bone formation, vascularisation and intramembranous ossification of the critical size calvarial defect were accelerated by using mesenchymal stem cells combined 3D spiral-wounded electrospun matrices.

ARTICLE HISTORY

Received 19 December 2018
Accepted 30 January 2019

KEYWORDS

Bone regeneration; cranial defects; mesenchymal stem cells; electrospinning; scaffold





Introduction

Bone is an active and vascularized connective tissue, which supports and protects the remaining systems and organs of the body. Even though having self-healing ability, the body cannot repair the large bone defects caused by aging, bone fractures, traumas, tumors, surgery and genetic diseases, which makes the bone second most transplanted tissue globally. Thus, millions of bone grafts and substitute materials are transplanted in surgical operations to the patients for the treatment of bone defects every year [1–3].

Autologous, allogeneic and xenogeneic bone grafts are commonly used for bone healing in clinical practice. Nevertheless, there are still lots of limitations such as the risk of donor area morbidity, multiple surgical operations, immunogenic responses, infection and pathogen transmission risks [4,5]. To overcome the obstacles of the conventional bone grafts, alternative bone graft materials obtained via bone tissue engineering, which is a multidisciplinary field aiming to regenerate damaged or lost tissues/organs through

the association of cells, scaffolds and biological agents, have attracted considerable attention in last three decades [6–9].

Bone tissue engineering scaffolds are 3D structures that provide a proper environment for cell attachment, proliferation, differentiation, and new tissue regeneration [5]. Both synthetic and natural polymers possessing unique properties including biocompatibility, controlled biodegradation rate, non-toxic degradation products, large interconnected porosity, mechanical strength/durability, high surface-to-volume ratio, are good candidates for bone tissue engineering scaffolds [10,11]. Common natural polymers such as chitosan, chitin, cellulose, silk, alginate, gelatin, collagen, fibrinogen, elastin, and synthetic polymers including poly(glycolic acid) (PGA), poly(lactic acid) (PLA), copolymers of PLA and PGA (PLGA), poly-L-lactic acid (PLLA), poly(glycerol sebacate), poly-anhydrides, poly(ethylene glycol) (PEG), polycarbonates, polyurethane (PU), polymethylmethacrylate (PMMA), and polycaprolactone (PCL) are mainly used for fabricating scaffolds used in bone engineering applications [12–14].

CONTACT Nimet Bölgen  nimetbolgen@yahoo.com  Faculty of Engineering, Department of Chemical Engineering, Mersin University, Ciftlikkoy Campus, Mezitli, Mersin 33343, Turkey; İbrahim Vargel  ivargel@gmail.com  Faculty of Medicine, Department of Plastics and Reconstructive Surgery, Hacettepe University, Ankara 06230, Turkey.

*Correspondence for in vivo study.

© 2019 The Author(s). Published by Informa UK Limited, trading as Taylor & Francis Group.

This is an Open Access article distributed under the terms of the Creative Commons Attribution License (<http://creativecommons.org/licenses/by/4.0/>), which permits unrestricted use, distribution, and reproduction in any medium, provided the original work is properly cited.

Among the FDA-approved synthetic polymers, PCL is a well-reputed biodegradable and biocompatible polymer used as a scaffold in bone tissue engineering applications due to its unique mechanical and chemical properties such as low melting point (59–64 °C) and good solubility. The semi-crystalline nature and hydrophobicity of PCL decrease the degradation rate and under the stress, PCL has the ability to resist shear flow and strain linearly with time, which make it an excellent candidate for using as long-term implants and tissue engineering scaffolds [14,15].

A broad range of scaffolds has been prepared by using different methods including freeze drying, rapid prototyping, fiber bonding, solvent casting, gas foaming, thermally induce phase separation, melt moulding, wet spinning and electrospinning. Electrospinning is a simple, yet versatile fabrication technique in order to obtain matrices with interconnected pore structure having a diameter from nano- to micrometer scale by applying a high voltage between the solution and the collecting target. In the last two decades, electrospun scaffolds gained great interest globally due to its flexibility, cost-effectiveness, ease of use, ability to align structures and control the diameters of the fibers [7,16,17].

Many different cell types including primary human bone and periosteal cells and stem cells play a crucial role in the bone regeneration process. Especially, mesenchymal stem cells (MSCs), which have osteogenic differentiation capability, are promising candidates for bone regeneration therapies due to their easy isolation from different tissues, rapid proliferation, unique immunomodulatory properties [18–20]. Researchers have developed a range of MSCs-based electrospun scaffolds possessing highly interconnected pore architecture with the nano- and microscale size, which provide good interaction between the MSCs and fibrous scaffolds. Moreover, several studies showed that microporosity plays a significant role in improving the osteogenesis of the scaffolds in bone repair process [21–23].

In this study, we spiral-wounded electrospun poly(ϵ -caprolactone) (PCL) membranes to obtain 3D scaffolds with nanofibers and macrochannels. Bone marrow mesenchymal stem cells isolated from Sprague Dawley rats were injected into the scaffolds after implantation in the cranial bone defects in rats. New bone formation, vascularization and intramembranous ossification of the critical size calvarial defect were investigated by using stem cells combined 3D spiral-wounded electrospun matrices.

Materials and methods

Preparation of 3D electrospun matrices

Poly(ϵ -caprolactone) (PCL) was synthesized from ϵ -caprolactone (Sigma-Aldrich, Germany) in a glass reactor under a nitrogen atmosphere for 24 h at 120 °C [24]. Stannous octoate (Sigma-Aldrich, USA) was used as a catalyst. The molar ratio of ϵ -caprolactone/stannous octoate was 1700:1 and 1700:3, for the synthesis of high- and low-molecular-weight polymers, respectively. The electrospinning solution containing high and low molecular PCL (20:80, wt) was prepared in a mixture of chloroform and dimethylformamide

(50:50, v) (Sigma-Aldrich, Germany). The total polymer concentration in the solution was 40 g/100 ml. The polymer solution was electrospun by using a high-voltage power supply (Gamma HVPS-ES40, USA), with an applied electrical field of 15 kV. The tip to capillary distance was 10 cm. The electrospun membranes were spiral-wounded to form cylindrically shaped scaffolds with a diameter of 8 mm, stuck using a tissue glue (G.R.F., MICROVAL, France) and cut into pieces with a height of 2 mm. The polymerization procedure, electrospinning system and the preparation of 3D matrices were described in detail in our previous study [16].

Preparation of rat bone marrow mesenchymal stromal/stem cells (MSC)

Under general anaesthesia, femur and tibia bones were obtained from Sprague Dawley rats. Bone samples were flushed and cells were centrifuged at 1500 rpm for 5 min and washed twice. Cells were plated in 75-cm² petri dishes at 3×10^5 cells/cm² concentration in DMEM-LG, in 20% FBS (Fetal Bovine Serum) (Sigma, Germany), 1% penicillin/streptomycin, and 2 mM glutamine (Sigma, Germany) and incubated at 37 °C and 5% CO₂. Medium changes were done in every 3–4 days. Confluent cells were detached by using 0.25% Trypsin/EDTA (Sigma, Germany) and counted manually with trypan blue [25]. Centrifuged cells pelleted and suspended in PBS to a final concentration of 1×10^6 cells per 50 μ L and transferred to insulin injectors for *in vivo* experiments. Osteogenic differentiation capacity of cells was tested by the use of differentiation media consisting of DMEM-LG, FBS, dexamethasone (Sigma, Germany), beta-glycerophosphate (Sigma, Germany) and ascorbic acid (Sigma, UK). Osteogenic differentiation was confirmed by Alizarin Red S staining at 21 days of culture. Extracellular matrix calcification was evident by the appearance of calcium deposits in culture. Images were obtained by Olympus microscope CKX41 (Tokyo, Japan).

Animal model

This study was carried out after the animal research protocol was approved by the Animal Ethical Committee of Hacettepe University (Approval number: 2007/29–11, Approval date: 26.03.2007). A total of 30 adult Sprague Dawley rats (body weight: 250–300 g) were included in this study. The animals were housed in a temperature and humidity controlled rooms with a 12-h light/dark cycle. Animals had free access to food and water and fed with standard rodent chow diet, *ad libitum*. A sterile surgical technique was applied throughout the study. The 3D electrospun spiral-wounded matrices were sterilized by ethylene oxide sterilization. Animals were anaesthetized by intraperitoneal injection of a mixture of ketamine HCl (Parke Davis, 50 mg/ml, Taiwan) and Rompun (Bayer, 2%, 50 ml, Germany). The implantation region of the test animal was shaved and disinfected with Baticon solution (Droksan, 10%, Turkey). The periosteum on the cranial surface was carefully cut and pulled to one side of the defect. 8 mm diameter of the cranial bone was removed by using a circular

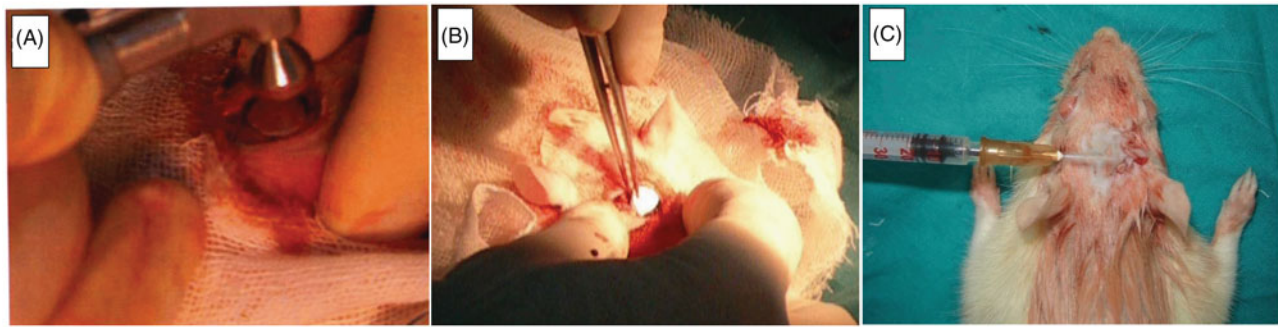


Figure 1. *In vivo* model: (A) Removal of cranial bone, (B) implantation of scaffold, (C) injection of stem cell suspension.

saw [26] (Figure 1(A)). The 3D electrospun spiral-wounded matrix was placed in the defect and the periosteum was put back to its original position (Figure 1(B)), and the incision was closed by suturing. 1×10^6 cells were incorporated inside the electrospun 3D matrices by injection after the incision was closed (Figure 1(C)). The dura mater and periosteum were kept intact. Twenty-eight animals were used to implant stem cells injected electrospun matrices. Cranial defects created by removing 8 mm diameters of the cranial bone of rats are critical-sized which means that they can not regenerate by themselves [27]. We also validated this result from our previous study [16]. Previously, we demonstrated the bone defect healing scores of an animal group without any implantation [16]. In this study, we analyzed the new bone/total cavity ratio, osteoblast lined active bone length and blood vessel density of the referred group without any implantation. We compared the results of histological analyses of the scaffold-stem cell implanted group with the results of the mentioned group without any implantation that served as control. The test animals were sacrificed after 30, 90 and 180 days of postimplantation, and soft and hard tissue specimens were removed and placed in 10% phosphate-buffered formalin (pH 7.0) at room temperature for fixation. All the samples were analyzed histologically. 180-day results of scaffold-stem cell implanted regions were analyzed first by X-ray Micro-computed tomography (microCT) and then using standard histology.

Histology and histomorphometry

Bones were fixed in 10% neutral buffered formalin at room temperature and 180-day specimens sent to microcomputed tomography. After microCT imaging, all specimens were decalcified in De Castro solution (chloral hydrate, nitric acid, distilled water), dehydrated in a graded series of ethanol and embedded in paraffin by using an automated tissue processor with vacuum. From each specimen block, 4- to 5- μm -thick serial sections were obtained using a sliding microtome (HM 430; Thermo Fisher Scientific, Munich, Germany). Sections were stained with hematoxylin and eosin (HE) and Masson's trichrome (MT) and evaluated for bone defect healing and tissue response to graft. Note that MT produces high contrast images with red (bone), green (osteoid-cartilage) and purple (cell cytoplasm). Stained sections were examined in a random and blinded manner by two investigators using a light microscope

(Leica DMR) attached with a computerized digital camera (Model DFC 480, Leica Westlar Germany). Bright-field images were captured and analyzed quantitatively by image processing program (Qwin Plus, Leica Inc. Westlar Germany). The number of pixels corresponding to a new trabecular bone area in each image was quantified, divided by the total number of pixels corresponding to the total defect area and converted to μm^2 in each specimen. Osteoblasts were quantified based on their morphology on HE-stained sections for a length of their linear apposition along osteoid-new bone surfaces relative to total new bone-osteoid surface length for 3 randomly selected high power fields (200 \times) and are reported as a fraction (%) average for each sample. New blood vessels within the defect were similarly digitally counted at four randomly selected high power fields (200 \times) and are reported as average for each sample [28,29]. A total tissue response score was given to each specimen regarding the presence of fibrous connective tissue formation and inflammatory cellular infiltration (Table 1) [16].

MicroCT analysis

Analyses were performed on cell-scaffold samples on day 180, using X-ray microcomputed tomography ($\mu\text{-CT}$, Skyscan1174, Belgium) in order to quantify mineralized matrix formation within the defect area, as an indicator of new bone formation [30–34]. The scanning conditions were 50 kV, 800 μA , a pixel size of 33 μm , beam hardening correction of 20%, a smoothing of 1, and ring artifact correction of 3. Scanning was performed by 360 $^\circ$ rotation, exposure time of 2500 ms, a rotation step of 0.7 $^\circ$, and frame averaging of 4. In all scans, flat field correction, geometric correction and random movement correction were performed [35–38]. The screening procedure took approximately 50 min per sample. Digital data were reconstructed using the NRecon software (Bruker micro-CT). CTAn software (Bruker micro-CT) was used for quantitative measurements of samples. Total defect and new bone volumes (mm^3) were measured and new bone was calculated for the total bone defect. Defect volume three-dimensional visualization and qualitative evaluation were performed with CTVol software (Bruker micro-CT).

Statistical analysis

Independent variables were the groups and the dependent variables were the histology and microCT parameters. The

Table 1. Tissue response scores.

Category	Parameters	Scores				
		4	3	2	1	0
Tissue response	Fibrous connective tissue formation	severe deposition of dense collagenous connective tissue around the implant.	disruption of normal tissue architecture and the presence of moderately dense fibrous connective tissue	presence of moderate connective tissue	presence of delicate spindle-shaped cells or mild fibroplasia	no difference from normal control tissue, no presence of connective tissue at or around the implant site
	Inflammatory cellular infiltration	severe cellular infiltrate response to an implant or tissue necrosis at or around the site	presence of large numbers of lymphocytes, macrophages and foreign body giant cells, also a notable presence of eosinophils and neutrophils	for the presence of several lymphocytes, macrophages with a few foreign body giant cells and small foci of neutrophils	presence of a few lymphocytes or macrophages, no presence of foreign body giant cells, eosinophil or neutrophils	no difference from normal control tissue, no presence of macrophages, foreign body cells, lymphocytes, eosinophils or neutrophils at or around the implant site

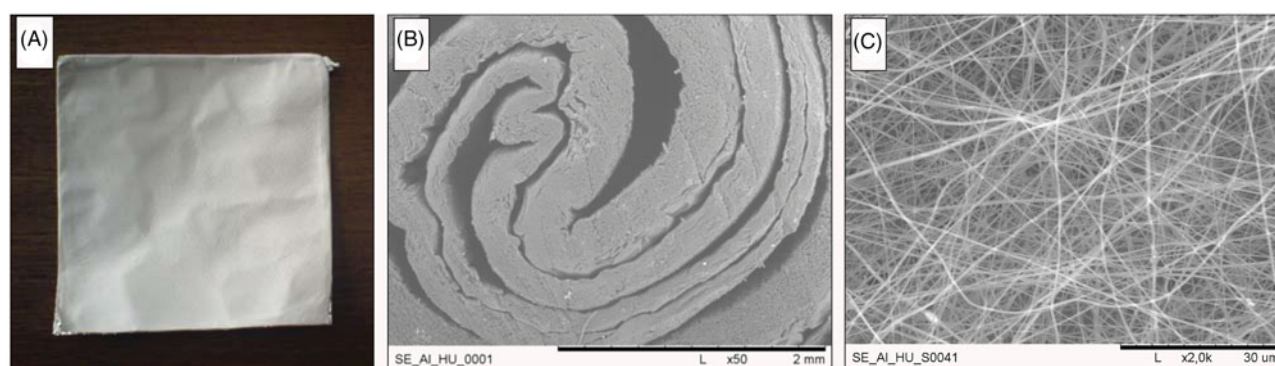


Figure 2. (A) Macroscopic image of PCL membrane, (B) SEM image showing the macrochannels of the spiral wound scaffold, (C) SEM image showing the nanofibrous structure of the PCL scaffold.

normality of distribution and the homogeneity of variances of the sample were established using the Shapiro–Wilk test. All parameters were analyzed by nonparametric tests, Kruskal–Wallis was used for multiple comparisons and Mann–Whitney U as *post hoc* test. Correlation between the histologic and microCT measurements was assessed by using Spearman test. Descriptive statistical values were expressed as median, minimum and maximum. The difference was considered significant if $p < .05$.

Results and discussion

Scaffold properties

PCL with two molecular weights (high and low) was successfully electrospun from its solution (Figure 2(A)). One of the drawbacks of electrospun membranes is their two-dimensional structure which is a limitation for 3D applications and pore size in nanometer scale which is lower than a cellular size that cannot allow cell migration. In order to overcome these drawbacks, we spiral-wounded electrospun membranes to prepare 3D matrices with macrochannels that would guide bone regeneration (Figure 2(B)), still including nanofibers (Figure 2(C)) that biomimic the structure of the connective tissues. 3D electrospun nanofibrous matrices with macrochannels were combined with stem cells and used in an approach for regeneration of cranial bone defects.

Histological evaluation

Micrographs of calvarial defect area bounded by compact bone are presented in Figure 3. New bone formation is observed in the macrochannels of the electrospun 3D scaffold. On day 90, the intramembranous ossification area with vascularity was observed in the center of the cavity (Figure 3(E)). Bone spicule was observed in the center of the cavity on day 180 (Figure 3(F)).

New bone per total defect area ratio was significantly higher in scaffold-stem cell implanted region comparing to the defects without any implantation at all time periods (day30, 90 and 180, $p < .05$) (Figure 4(A)). Stem cell-scaffold implanted regions had higher new blood vessel number near the implant compared to the defect area without implantation at all time points ($p < .05$) (Figure 4(B)). New bone trabecules lined by active bone-forming cells (osteoblasts) were higher in the scaffold-stem cell implanted region compared to the empty cavities without implantation at all time periods ($p < .05$) (Figure 4(C)). New bone/total cavity ratio, osteoblast-lined active bone length and blood vessel density increased with time. According to this data new bone formation and vascularisation were accelerated in scaffold-stem cell implanted defects at all time points.

Tissue response scores remained low with a mild tissue response to the implant (Figure 4(D)). Within its empty channels, the polymer allowed a guided new bone formation from

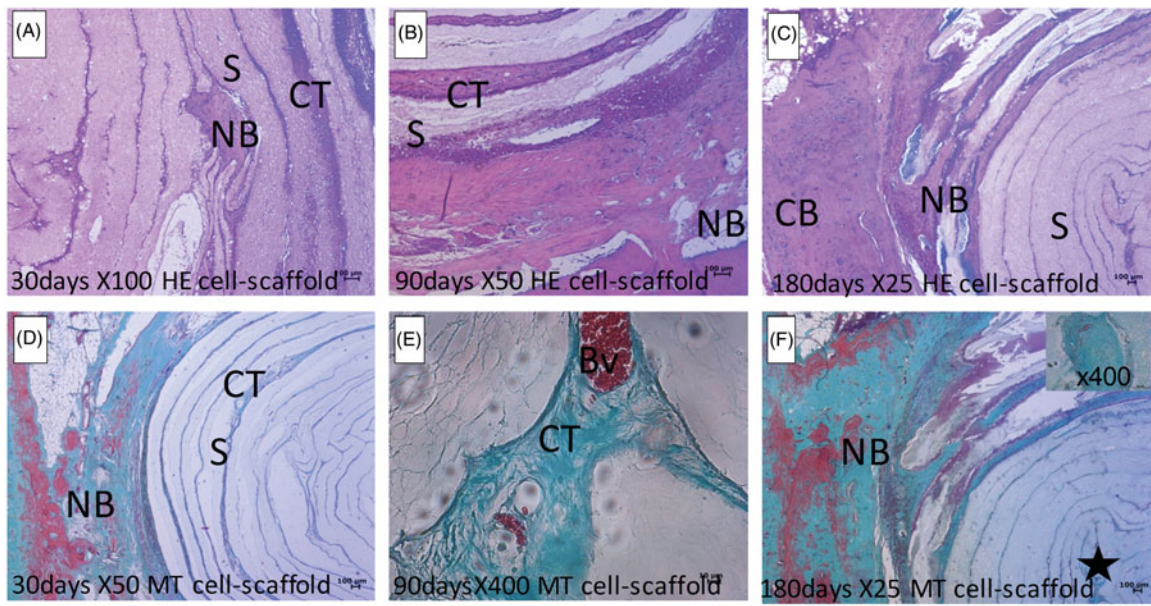


Figure 3. Representative photomicrographs of the scaffold-stem cell groups demonstrating the defect area surrounded by compact bone. Left column (A, D), middle column (B, E) and right column (C, F) show 30, 90 and 180 days, respectively. F inset shows the bone spicule (indicated by a star) at the center of the cavity. CB: Compact bone; NB: New bone; BD: Connective tissue; S: Scaffold; Bv: Blood vessel; HE: Haematoxylin & Eosin; MT: Masson's Trichrome.

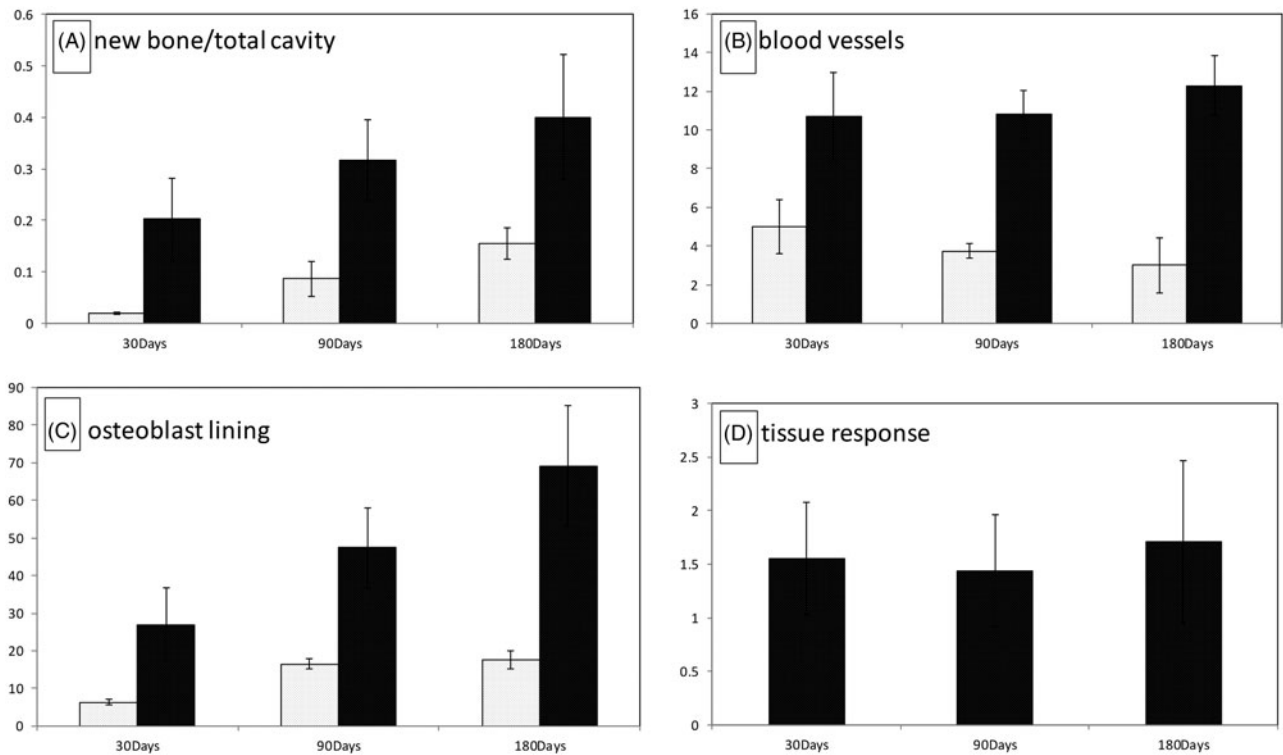


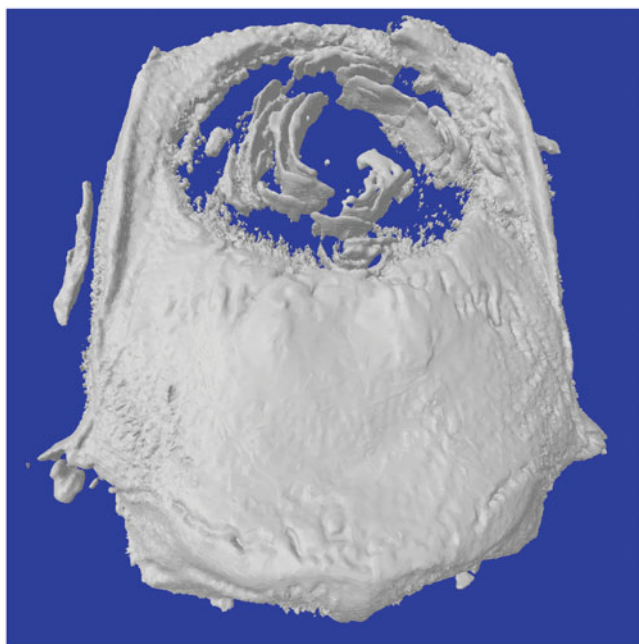
Figure 4. (A) New bone per total defect area ratio, (B) new blood vessel number, (C) osteoblast lining, (D) tissue response scores.

both peripheric and central regions of the cavity. The scaffold-stem cell combined biomaterial was biocompatible, since neither fibrosis (scar tissue), nor necrosis, nor foreign body reaction were detected in any of the samples at any time point. Polymer started to degrade minimally peripherally towards the center on day 30. However, the electrospun 3D matrice kept

its circular shape and continue to guide the remodeling of new bone trabecules in its channels until day 180. None of the cavities were totally ossified on day 180. According to this data, the electrospun 3D matrice was biocompatible and scaffold-stem cell combined biomaterial accelerated intramembranous ossification of the critical size calvarial defect.

Table 2. MicroCT results.

Sample number	Total defect volume (mm ³)	New bone volume (mm ³)	New bone volume/total defect volume (%)
1	157.977271	18.31390735	11.59275
2	113.1462004	6.940962952	6.13451
3	142.4618446	13.96349183	9.80157
4	127.3373865	7.286718153	5.72237
5	138.8037724	10.63930423	7.66500
6	113.0693617	12.60229822	11.14563
7	100.1948763	7.106975738	7.09315

**Figure 5.** A representative microCT image of cell-scaffold samples on day 180.

MicroCT results

Mineralized matrix formation within the defect area, as an indicator of new bone formation, was quantified by microCT. Total defect and new bone volumes (mm³) were measured, and new bone to total defect volume was calculated (Table 2). According to the results, the average new bone/total defect volume was calculated as $8.45 \pm 2.38\%$. This result was compared to the result of histologic analysis (new bone/total cavity percentage was $40.05 \pm 12.01\%$).

New bone/total cavity measured by microCT was found to be lower than the measured value by histology. Because, only mineralized bone tissue could be measured by microCT, and the histological measurement included both the mineralized bone tissue and bone progenitors that did not mineralize yet. However, the result of microCT was parallel to histology analysis, in demonstrating the ossification in the macro-channels of the 3D electrospun scaffold starting from the center (Figure 5).

Conclusion

The cranial region is composed of bones, which are non-load bearing and have membranous bone histology. Besides, calvarial bones have a biological microenvironment with high osteogenic potential, since they are surrounded by periost on

the upper side and dura mater on the lower side. The osteoblastic activity is supposed to be at the optimum level in this biologic microenvironment. In clinics, the expectation of self-healing of the cranial bone defects over a critical size is very low. Beside insufficiency of the vascularization level, inadequate cell and signal pathways that play a role in the osteoblastic phase are claimed to be reasons of low self-healing capacity of defected cranial bones. Calvarial bone defects of paediatric patients heal spontaneously if the size of the defect is lower than a critical size. However, the same sized calvarial defects of geriatric patients can not heal spontaneously. These clinical observations/findings prompted the researchers to search the effects of stem cells combined scaffolds on the induction of bone regeneration. The scaffold that has similar properties with the original tissue and the cells which have functional properties play an important role in the repair of bone defects. Growing research focused on the design of scaffolds that simulate the natural bone from nano to micrometer scale to enhance the interaction between scaffold, cells and the microenvironment. Stem cells within the other source of cells are known to have better regeneration capacity and they differentiate into various type of cells, leading to being used in bone tissue engineering. In this study, macrochanneled scaffolds including nanofibers in their structure were combined with mesenchymal stem cells in order to repair cranial bone defects. Mineralization was observed in the macro channelled nanofibrous scaffold. It was not only observed in the peripheral region of the scaffold, but also observed in the centre. New bone formation and vascularization was observed in the cavity. The synergy of the morphologic structure of the scaffold and the mesenchymal stem cells may have resulted in the new bone formation in the cranial defect. This study reports a preliminary approach to develop an efficacious stem cell-scaffold material which can be used in cranial bone tissue engineering applications with compatible physical characteristics of natural bone, including nanofibers and macrochannels.

Acknowledgement

This study was performed in the context of the EU-FP6-NoE Expertissues Project. Erhan Pişkin is supported by Turkish Academy of Sciences as a Honorary Member. This study was a part of PhD thesis of İsmail Alper İšoğlu. The thesis was supervised by Erhan Pişkin.

Disclosure statement

No potential conflict of interest was reported by the authors.

References

- [1] Neto A, Ferreira J. Synthetic and marine-derived porous scaffolds for bone tissue engineering. *Materials* (Basel). 2018;11:1–40.
- [2] Pearlín, Nayak S, Manivasagam G, Sen D. Progress of regenerative therapy in orthopedics. *Curr Osteoporos Rep*. 2018;16:169–181.
- [3] Turnbull G, Clarke J, Picard F, et al. 3D bioactive composite scaffolds for bone tissue engineering. *Bioact Mater*. 2018;3:278–314.
- [4] Zhang D, Wu X, Chen J, et al. The development of collagen based composite scaffolds for bone regeneration. *Bioact Mater*. 2018;3:129–138.
- [5] Dang M, Saunders L, Niu X, et al. Biomimetic delivery of signals for bone tissue engineering. *Bone Res*. 2018;6:25.
- [6] Guo B, Ma PX. Conducting polymers for tissue engineering. *Biomacromolecules*. 2018;19:1764–1782.
- [7] Jun I, Han H-S, Edwards J, et al. Electrospun fibrous scaffolds for tissue engineering: viewpoints on architecture and fabrication. *IJMS*. 2018;19:745.
- [8] Goonoo N, Bhaw-Luximon A. Regenerative medicine: induced pluripotent stem cells and their benefits on accelerated bone tissue reconstruction using scaffolds. *J Mater Res*. 2018;33:1573–1591.
- [9] Attia AC, Yu T, Gleeson SE, et al. A review of nanofiber shish kebabs and their potential in creating effective biomimetic bone scaffolds. *Regen Eng Transl Med*. 2018;4:107–119.
- [10] Al-Enizi A, Zagho M, Elzatahy A. Polymer-based electrospun nanofibers for biomedical applications. *Nanomaterials*. 2018;8:259.
- [11] Winkler T, Sass FA, Duda GN, et al. A review of biomaterials in bone defect healing, remaining shortcomings and future opportunities for bone tissue engineering. *Bone Joint Res*. 2018;7:232–243.
- [12] De Witte T-M, Fratila-Apachitei LE, Zadpoor AA, et al. Bone tissue engineering via growth factor delivery: from scaffolds to complex matrices. *Regen Biomater*. 2018;5:197–211.
- [13] Fernandez de Grado G, Keller L, Idoux-Gillet Y, et al. Bone substitutes: a review of their characteristics, clinical use, and perspectives for large bone defects management. *J Tissue Eng*. 2018;9:204173141877681.
- [14] Mkhabela VJ, Ray SS. Poly(ϵ -caprolactone) nanocomposite scaffolds for tissue engineering: a brief overview. *J Nanosci Nanotech*. 2014;14:535–545.
- [15] Hajiali F, Tajbakhsh S, Shojaei A. Fabrication and properties of polycaprolactone composites containing calcium phosphate-based ceramics and bioactive glasses in bone tissue engineering: a review. *Polym Rev*. 2018;58:164–207.
- [16] Pişkin E, İşoğlu IA, Bölgen N, et al. *In vivo* performance of simvastatin-loaded electrospun spiral-wound polycaprolactone scaffolds in reconstruction of cranial bone defects in the rat model. *J Biomed Mater Res*. 2009;90A:1137–1151.
- [17] Zhao P, Gu H, Mi H, et al. Fabrication of scaffolds in tissue engineering: a review. *Front Mech Eng*. 2018;13:107–119.
- [18] Moradi SL, Golchin A, Hajishafieeha Z, et al. Bone tissue engineering: adult stem cells in combination with electrospun nanofibrous scaffolds. *J Cell Physiol*. 2018;233:6509–6522.
- [19] Almalki SG, Agrawal DK. Key transcription factors in the differentiation of mesenchymal stem cells. *Differentiation*. 2016;92:41–51.
- [20] Gao F, Chiu SM, Motan DAL, et al. Mesenchymal stem cells and immunomodulation: current status and future prospects. *Cell Death Dis*. 2016;7:e2062.
- [21] Zhang K, Fan Y, Dunne N, et al. Effect of microporosity on scaffolds for bone tissue engineering. *Regen Biomater*. 2018;5:115–124.
- [22] Wang S, Hu F, Li J, et al. Design of electrospun nanofibrous mats for osteogenic differentiation of mesenchymal stem cells. *Nanomed Nanotechnol Biol Med*. 2018;14:2505–2520.
- [23] Preethi Soundarya S, Sanjay V, Haritha Menon A, et al. Effects of flavonoids incorporated biological macromolecules based scaffolds in bone tissue engineering. *Int J Biol Macromol*. 2018;110:74–87.
- [24] Senköylü A, Ural E, Kesenci K, et al. Poly(D, L-lactide/epsilon-caprolactone)/hydroxyapatite composites as bone filler: an in vivo study in rats. *Int J Artif Organs*. 2002;25:1174–1179.
- [25] Ayatollahi M, Salmani MK, Geramizadeh B, et al. Conditions to improve expansion of human mesenchymal stem cells based on rat samples. *World J Stem Cells*. 2012;4:1–8.
- [26] Bölgen N, Korkusuz P, Vargel İ, et al. Stem cell suspension injected HEMA-lactate-dextran cryogels for regeneration of critical sized bone defects. *Artif Cells, Nanomed, Biotechnol*. 2014;42:70–77.
- [27] Burdick JA, Frankel D, Dernel WS, et al. An initial investigation of photocurable three-dimensional lactic acid based scaffolds in a critical-sized cranial defect. *Biomaterials*. 2003;24:1613–1620.
- [28] Lu M, Rabie AB. Quantitative assessment of early healing of intramembranous and endochondral autogenous bone grafts using micro-computed tomography and Q-win image analyzer. *Int J Oral Maxillofac Surg*. 2004;33:369–376.
- [29] Petrie Aronin CE, Sadik KW, Lay AL, et al. Comparative effects of scaffold pore size, pore volume, and total void volume on cranial bone healing patterns using microsphere-based scaffolds. *J Biomed Mater Res*. 2009;89:632–641.
- [30] Jaecques SVN, Van Oosterwyck H, Muraru L, et al. Individualised, micro CT-based finite element modelling as a tool for biomechanical analysis related to tissue engineering of bone. *Biomaterials*. 2004;25:1683–1696.
- [31] Schantz JT, Teoh SH, Lim TC, et al. Repair of calvarial defects with customized tissue-engineered bone grafts I. Evaluation of osteogenesis in a three-dimensional culture system. *Tissue Eng*. 2003;9:113–126.
- [32] Schantz JT, Huttmacher DW, Lam CFX, et al. Repair of calvarial defects with customised tissue-engineered bone grafts ii. Evaluation of cellular efficiency and efficacy *in vivo*. *Tissue Eng*. 2003;9:127–139.
- [33] Meinel L, Karageorgiou V, Hofmann S, et al. Engineering bone-like tissue in vitro using human bone marrow stem cells and silk scaffolds. *J Biomed Mater Res A*. 2004;71:25–34.
- [34] Tuan HS, Huttmacher DW. Application of micro CT and computation modeling in bone tissue engineering. *Comput Des*. 2005;37:1151–1161.
- [35] Bayram HM, Bayram E, Ocak M, et al. Effect of ProTaper gold, self-adjusting file, and XP-endo shaper instruments on dentinal microcrack formation: a micro-computed tomographic study. *J Endod*. 2017;43:1166–1169.
- [36] Yılmaz F, Koç C, Kamburoğlu K, et al. Evaluation of 3 different retreatment techniques in maxillary molar teeth by using micro-computed tomography. *J Endod*. 2018;44:480–484.
- [37] Küçükçaya Eren S, Aksel H, Askerbeyli Örs S, et al. Obturation quality of calcium silicate-based cements placed with different techniques in teeth with perforating internal root resorption: a micro-computed tomographic study. *Clin Oral Investig*. 2019;23:805–811.
- [38] Bayram HM, Bayram E, Ocak M, et al. Micro-computed tomographic evaluation of dentinal microcrack formation after using new heat-treated nickel-titanium systems. *J Endod*. 2017;43:1736–1739.